Materials Advances

PAPER

Check for updates

Spontaneous delamination of affordable natural vermiculite as a high barrier filler for biodegradable food packaging†

Volodymyr Dudko,‡[a] Renee L. Timmins,‡[a] Olena Khoruzhenko,[a] Maximilian Röhrl,[a] Christopher Greve, [c] Sabine Rosenfeldt,[a] Tekla Tammelin, [b] Seema Agarwal,[a] Eva M. Herzig [c] and Josef Breu *[a]

Expensive biodegradable packaging as a preventative measure against continued accumulation of plastic waste in our environment is often in conflict with the need for high performing packaging materials that prevent food waste. Compounding with delaminated vermiculite nanosheets is a compelling concept to simultaneously improve barrier properties through creation of a 'tortuous path' while also decreasing the price of the system due to its natural abundance. However, an effective delamination process that captures the full barrier improvement potential of this natural filler has been lacking. Here, we present a superior protocol for vermiculite delamination based on reducing the intrinsic hydrophobicity due to interlayer Mg^{2+} cations and the transfer of this osmotically swollen, liquid crystalline state into organic solvents. Nanocomposite coatings of degradable polyesters on nanocellulose exhibited oxygen and water transmission rates of 1.30 cm^3 m^{-2} day^{-1} atm^{-1} and 1.74 g m^{-2} day^{-1}, respectively, which competes with high-end, non-degradable poly(vinylidene dichloride) films.

Introduction

Innovative packaging plays a critical role in preventing loss of precious food products, yet presents a massive problem when considering their end-of-life scenarios. The United Nations Food and Agricultural Organisation estimates the global food wastage to be equivalent to 1.3 billion tons, which results in an unnecessary 3.3 billion tonnes of CO_2 equivalent of greenhouse gases being released into the atmosphere per year.[1] Materials like polyethylene, poly(vinylidene dichloride) (PVDC), and polyamide possess a high barrier to relevant permeants, including water vapour, carbon dioxide, and oxygen, which prevents food waste by protecting from contamination and preserving freshness, taste, and colour of the products. Despite these critical functions, the growing concerns and awareness of consumers towards plastic pollution and ubiquitous microplastic contamination was reflected in a major Ipsos poll conducted

in 2019, which found that 71% of global consumers believe that single use plastic products should be banned as soon as possible.[2] More recently, directives came from both the European Union and Canada to ban the use of certain single-use plastics,[3,4] spearheading a growing movement to replace traditional plastics with biodegradable alternatives in the interest of environmental preservation and human health.[5,6] Current coated and chemically treated paper alternatives only present an unrecyclable and non-compostable burden on waste management systems.[7] There still lacks an environmentally friendly packaging option that provides the lightweight and convenient protection to which we have become accustomed.

Accordingly, one must consider the overall environmental impact of a packaged food product including the life cycle of the packaging material as well as the food. Implementation of bio-based and biodegradable packaging is an important step, but without high-performance properties that reduce food waste, the net environmental impact of the entire system is not improving.[8] Moreover, most consumers are unwilling to pay a higher price for an item to have environmentally friendly packaging.[9] A material substitution may become more attractive as the cost of certain biobased materials, *e.g.* cellulose and cellulose-based materials, decreases with increased production volumes while the rising price of petroleum threatens the rock-bottom price tag of conventional polymers.[10] Practical and low cost solutions required to tackle the challenge of the poor and

[a] *Bavarian Polymer Institute and Department of Chemistry, University of Bayreuth, Universitätsstr. 30, 95440 Bayreuth, Germany. E-mail: Josef.Breu@uni-bayreuth.de*

[b] *VTT Technical Research Centre of Finland Ltd, VTT, PO Box 1000, FI-02044 Espoo, Finland*

[c] *Physikalisches Institut, Dynamik und Strukturbildung-Herzig Group, Universität Bayreuth, Universitätsstr. 30, 95447 Bayreuth, Germany*

moisture susceptible barrier properties of these bio-based and biodegradable materials are through multilayer strategies or surface hydrophobisation strategies.[11–13] These methods indeed decrease moisture sensitivity of hydrophilic materials, but still fails to provide barrier levels acceptable for food packaging. Another such approach is by the application of a thin nanocomposite barrier coating using clay nanosheets. Nanocomposite foils have barrier performance improved by orders of magnitude compared to the neat substrate.[14–16] The use of natural clays offers the additional benefit of being an inexpensive and sustainable filler that reduces the overall cost of the packaging.

As barrier improvement scales with the square of the platelet aspect ratio (diameter/thickness ratio) due to elongation of the diffusion path for permeates,[17] the most commonly applied clay minerals, montmorillonite and LAPONITE®[18,19] with an aspect ratio of < 150 and 20, respectively, are insufficient. Particularly when considering the inherently poor barrier performance of biodegradable polymer matrixes,[19,20] much larger aspect ratios are required. Layered fillers with promising diameters are synthetic hectorites[21] or natural vermiculites. While efficient delamination protocols for the former have already been established (*i.e.*, osmotic swelling),[21] the same cannot be said for the latter.

Osmotic swelling[22] is an exceptionally effective method for the production of barrier nanosheets since it is a thermodynamically allowed process that does not require any mechanical force as opposed to ultrasound driven liquid-phase exfoliation methods. Being repulsive[23,24] in nature allows for an utter and most gentle delamination into the thinnest possible nanosheets, while liquid phase exfoliation provides only nanosheets with a range of thicknesses (for a definition of delamination *versus* exfoliation, see: Gardolinsky and Lagay).[25] Consequently, only delamination *via* osmotic swelling preserves the aspect ratio inherent in the platelet diameter of the non-delaminated starting material.

Considering the polymer component of a nanocomposite coating, commercially produced biodegradable polymers like poly lactic acid (PLA), poly(butylene succinate-*co*-butylene adipate) (PBSA), and poly(butylene adipate terephthalate) (PBAT) are attractive options, but only soluble in organic solvents. Until recently, osmotic delamination was restricted to a very small number of layered compounds in water.[26–30] Water soluble biodegradable polymers like poly(vinyl alcohol) (PVOH) are highly susceptible to swelling even under ambient conditions, significantly deteriorating the barrier performance.[31,32] Fortunately, osmotic swelling of a synthetic hectorite could recently be extended into applicable organic solvents.[33]

Natural vermiculites are 2 : 1 layered silicates are particularly appealing as a clay component in a nanocomposite barrier system, in contrast to a synthetic hectorite, because vermiculite deposits are abundant with global production at over 500 k tons per year[34] and cost around 20 ct per kg. Thermally expanded vermiculites are well-known in chemistry laboratories as the standard adsorbent for spilled organic solvents (Fig. 1a). Moreover, vermiculites have the same layer structure as the commonly applied montmorillonite but with a much larger diameter, and hence a higher potential aspect ratio.[35–37] Vermiculites unfortunately have a significantly higher charge density compared to montmorillonite, which renders osmotic swelling much more difficult.[38] Vermiculite swelling is not only impeded by the high charge density, but also by the dominant divalent interlayer cation Mg^{2+} that forms a strong and symmetrical electrostatic interaction with the adjacent nanosheets, pinning them together. Yet upon exchange with bulky organocations, vermiculite is known to swell osmotically in water.[39–42] Due to the large diameter of nanosheets, gels obtained by swelling are not isotropic but rather viscous, liquid crystalline, nematic phases even at low concentrations of 1 vol%. It follows that in order to efficiently incorporate vermiculite into a biodegradable polymer matrix for use in sustainable food packaging, obtaining osmotic swelling in organic solvents is a critical hurdle. More specifically, for solution casting in a roll-to-roll production of nanocomposite coatings, osmotic swelling of vermiculite is required in a solvent that also dissolves biodegradable polyesters.

In this paper, we report a simple one-step ion exchange strategy for repulsive osmotic delamination of natural vermiculite in the organic solvent *N*-methyl formamide (NMF) and its mixtures that results in a high delamination yield (80 wt%) and preservation of the high aspect ratio of the nanosheets compared to ultrasonication-assisted methods.[43] Solution blending with biodegradable polymers like PLA becomes straightforward. Nanocomposite coatings obtained by the doctor blading of a polymer/clay suspension improved gas barrier performance of a natural, fully biodegradable,[13] and highly hydroscopic wood-based nanocellulose paper substrate by 90.2% and 97.8%, respectively. The PLA-vermiculite coated nanocellulose system presents a biodegradable alternative to traditional high-performance food packaging with oxygen and water transmission rates of 1.30 cm^3 m^{-2} day^{-1} atm^{-1} and 1.74 g m^{-2} day^{-1}, respectively. Moreover, our manufacturing strategy involves only facile and scalable unit operations positively contributing to the future implementation at a commercial scale.

Results and discussion

Repulsive osmotic delamination of natural vermiculites

Osmotic swelling of highly charged clays occurs when the interlayer cation is completely exchanged for select bulky and hydrophilic organocations.[39–42] Cations are solvated by the solvent molecules, increasing the separation between nanosheets and boosting translational entropy within the interlayer space. Upon reaching a separation threshold, osmotic swelling sets in, allowing for a most gentle delamination process while preserving the aspect ratio inherent to the pristine platelet diameter.[23,24,38,44]

Vermiculites are the weathering products of biotite, where the K^+ cations are replaced by Mg^{2+} while at the same time the layer charge is reduced somewhat by oxidation of structural iron with oxygen in the air.[45] Due to the high hydration enthalpy of Mg^{2+}, vermiculites are hydrated. Hydration of
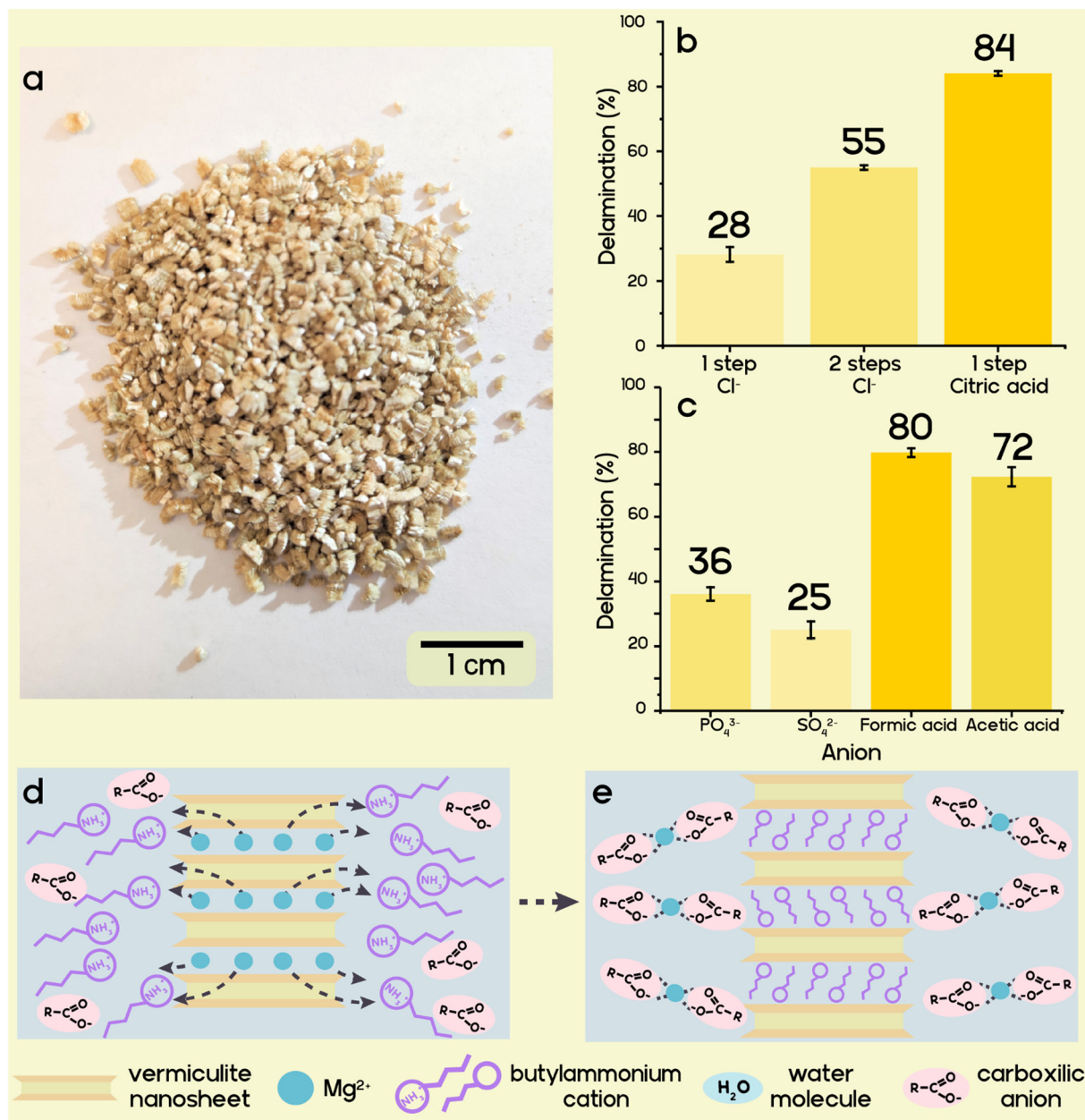
Fig. 1 Schematic representation of osmotic swelling of natural vermiculites. (a) Photo of thermally expanded natural vermiculite. (b) Delamination yield observed by a one-step ion exchange with butylammonium chloride or citrate as compared to a two-step ion exchange first to Na^+ followed by butylammonium chloride. (c) Delamination yield observed by a one-step ion exchange with different inorganic and organic salts of butylammonium. (d) Schematic of ion exchange process in presence of carboxylic acid anions (e). The proposed process of ion exchange that leads to enhanced delamination yield. Magnesium cations form complexes with carboxylic acid anions, increasing the hydrophilicity and reducing the tendency to re-enter the interlayer space.

pristine vermiculites, however, is limited to a two-layer hydrate even when immersed into water because of the high charge density. Owing to the natural origins of such vermiculites, contamination with pristine biotite mica impurities (which have an inaccessible interlayer space and do not exhibit any swelling behaviour) is inevitable. We cannot expect to achieve a 100% yield of delaminated nanosheets from the raw mined material because of this remaining accessory mineral.

Divalent interlayer cations like Mg^{2+}, as found in the pristine vermiculite, impede osmotic swelling. Complete exchange of divalent interlayer cations with monovalent cations of higher hydration energy (*e.g.*, Li^+)[46] or one capable of inducing steric pressure (*e.g.*, butylamine)[39] is essential for osmotic swelling to set in. The high selectivity in the interlayer space of vermiculite makes the direct and complete exchange of Mg^{2+} for Li^+ or protonated butylamine difficult and time-consuming. According to Walker *et al.*, butylamine vermiculites that produce gels upon swelling have been obtained by repeated ion exchange of Mg^{2+} with Na^+ over a period of one year.[40] Only then in a second step can Na^+ be sufficiently replaced by butylammonium. Needless to

say, such a lengthy two-step ion exchange process is unsuitable for high-volume applications.[39]

We hypothesise that by removing the Mg^{2+} cation from an exchange equilibrium through complexation, a high yield of ion-exchanged vermiculite in a single-step ion exchange is possible. Complexation is supplemented by the hydrophobicity of incoming organocations.[47] Carboxylic acids can be used for protonation of butylamine, while at the same time they can form stable complexes with Mg^{2+}, decreasing its activity to a level where butylammonium favourably enters the interlayer space. Vermiculite must first be activated for osmotic swelling by ion exchange in water. A series of ion exchanges were performed using butylamine in combination with one of several protonating acids to determine the most efficient paring for maximizing the yield of the nematic phase consisting of delaminated nanosheets, and to compare with the published two-step ion exchange (Fig. 1b and c).[40] Direct ion exchange with butylammonium chloride gives only 28 wt% delamination yield, while the two-step method involving sequential exchange of Mg^{2+} for Na^+, and then for butylammonium, provided a higher yield of 55 wt%. Butylammonium phosphate, sulfate, formate, and acetate produced yields of 36 wt%, 25 wt%, 80 wt%, and 72 wt%, respectively. The higher complex building constant for Mg^{2+} and the citrate anion compared to monodentate anions gives a superior yield of 84 wt% for butylammonium citrate (Fig. 1d and e).[48,49] Moreover, it was found that the concentration of the butylamine solution can be decreased 10-fold without a dramatic reduction of the delamination yield (from 84% at 1 M to 75% at 0.1 M, Fig. S1, ESI†). As high ionic strength hampers repulsive osmotic swelling, the delamination yields were determined after washing in ethanol followed by redispersion into water. CHN analysis of butylammonium citrate exchanged vermiculite confirms the highest organic content out of all exchanged vermiculites, which corresponds to 91% of the cation exchange capacity, indicating a high degree of ion exchange (Table S1, ESI†).

Characterization of nematic phases and delaminated vermiculite nanosheets

Coarse-grained, non-delaminated mica may be removed through sedimentation by centrifugation, which also gives a concentrated gel of delaminated vermiculite in the supernatant. The small-angle X-ray scattering (SAXS) (Fig. 2a red dots) of gel in NMF confirms the separation to the single layers to 62.8 nm (corresponding to $q = 0.01$ Å^{-1}). Nematic ordering is confirmed by the presence of a rational 00l series and an absence of Bragg reflexes at high q values (Fig. 2a red line), which would correspond to the swollen intercalation compound of 1.4 nm.[50] The pattern can be modelled with the disk shape structure factor (Fig. 2a blue dotted line) having a diameter of 2000 nm and thickness of 1.8 nm.[44,51,52]

Static light scattering (SLS) gave a mean particle size of about 4.9 µm (Fig. 2b), which corresponds to the hydrodynamic diameter of the nanosheets. Since SLS measurements were performed in aqueous dispersions, the particle size distribution is representative of the bulk material.[53] This value was cross-checked by assessing a large number of vermiculite nanosheets with SEM micrographs (Fig. 2c), which gave a mean diameter of 4 ± 1 µm, in agreement with the SLS value.

While SAXS probes the bulk suspension, delamination of vermiculite may be confirmed at the level of individual nanosheets with atomic force microscopy (AFM). The average height of three nanosheets was 1.2 ± 0.1 nm (Fig. 2d and Fig. S2, ESI†). Since AFM images were recorded under ambient conditions, counter ions attached to the basal surface will be solvated, which adds to the true thickness of 1 nm for a 2:1 layered material.[21] Taking this systematic error into account, it can safely be concluded that all imaged nanoplatelets are single layers because observed heights are significantly smaller than 2 nm.

Considering a nanosheet thickness of 1 nm and a 4 µm median lateral extension of the clay particles, delaminated natural vermiculite from Eucatex, Brazil offers a mean aspect ratio of 4000. This aspect ratio is more than an order of magnitude higher than the typical value for montmorillonite and is comparable to synthetic sodium tetrasilicic mica.[54] Such a high aspect ratio filler in a nanocomposite is expected to have a considerable impact on the barrier properties in combination with biodegradable polymers (Fig. S3 and eqn (S1), ESI†).

Nematic suspension of vermiculite in organic solvents

As most biodegradable polymers of commercial interest are non-water soluble polyesters (PLA, PBSA, PBAT, poly(ε-caprolactone)), the nematic aqueous vermiculite suspensions were freeze-dried before being re-suspended in organic solvents. Of the solvents tested, NMF proved to be capable of osmotic swelling butylammonium vermiculite yielding nematic suspensions. The greatest advantage of NMF over the other solvents is its exceptionally high dielectric constant ($\varepsilon_r = 171$).[55] Unfortunately, NMF has been reported to considerably reduce the molecular weight of PLA during dissolution, which in turn ruins the mechanical integrity of PLA composites.[16] Therefore, the suspension of vermiculite in NMF was concentrated by centrifugation to a gel with 9 wt% vermiculite. The gel is then diluted to 1 wt% with various other organic solvents yielding mixtures with less than 10 wt% NMF. Most low dielectric solvents instantly trigger flocculation. However, some moderately polar solvents that are used in the industrial coating preparation, including dimethylformamide (DMF), dimethylacetamide (DMac), dimethyl sulfoxide (DMSO), N-methyl-2-pyrrolidone (NMP), ethanol, and γ-butyrolactone (γ-BL), preserve the nematic nature of the vermiculite suspension as indicated by birefringence under cross-polarised light (Fig. 2e).

Out of the various solvent parameters evaluated, only a high dielectric constant displays a correlation with the stability of the liquid crystal phase (Table S2, ESI†). The only clear outliers are acetonitrile and ethanol, where the former has a lower dielectric constant than expected, but still induces swelling. Assuming the wt% of NMF to be 10%, the threshold value for the dielectric constant of a co-solvent in a solvent mixture appears to be 36. The flocculated samples are shown in Fig. S4 (ESI†).

The solubility of biodegradable polymers may be estimated by applying the Hansen parameters[56] (Table S2, ESI†). Out of the listed solvents capable of osmotic swelling, γ-BL has Hansen
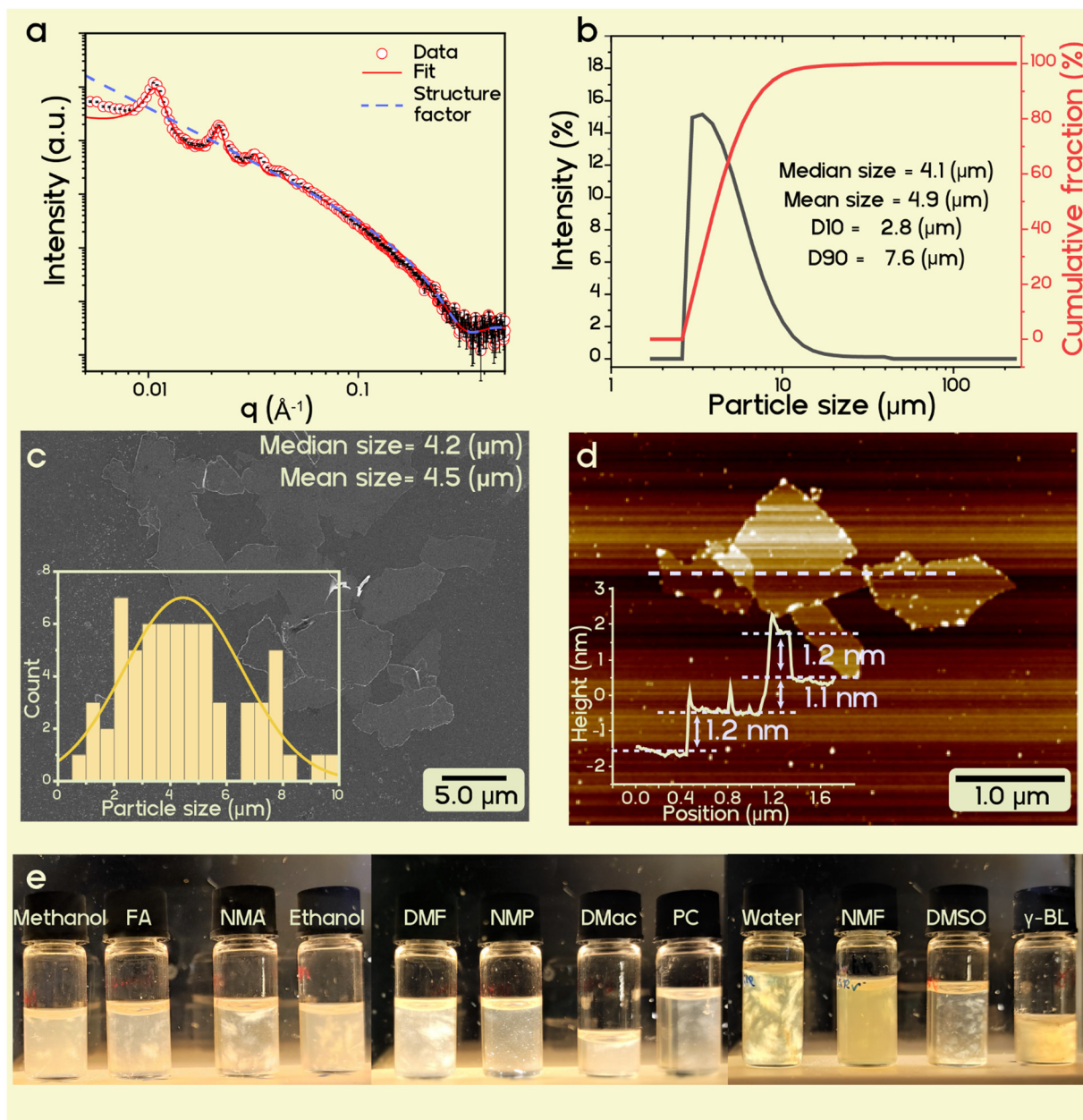
Fig. 2 Characterization of nematic suspensions and delaminated vermiculite nanosheets (a). SAXS intensity of vermiculite gel, indicating a liquid crystalline order in the nematic suspension in NMF. (b) Static light scattering number weighted size distribution indicating a mean size of 4.9 μm (c) SEM photo of vermiculite nanosheets on a Si wafer. Inset: Particle size distribution measured from the SEM image indicating a mean size of 4 ± 1 μm. (d) Topographic AFM image of vermiculite nanosheets and height profile from the single nanosheets indicating a height of ~1.2 nm. (e) Photos of nematic suspensions of vermiculite in various solvents obtained by diluting a vermiculite/NMF gel, viewed under cross-polarized light.and reducing the tendency to re-enter the interlayer space.

parameters which indicate that it will also be capable of dissolving biodegradable polyesters (Hansen parameters for PLA are 18.9, 4.6 and 7.6 MPa$^{1/2}$ for δD, δP, and δH, respectively), as required for the preparation of high-performance, degradable nanocomposites *via* solution blending and roll-to-roll processing.

Fabrication of biodegradable food packaging foils

Cellulose nanofiber (CNF) paper has recently been established as an inexpensive, wood-based, sustainable, and completely biodegradable substrate. Previous work has established the ability of this CNF substrate to degrade in compost within 4 weeks, which was comparable with other chemically unmodified cellulose variants.[13,57,58] The CNF paper used, which was prepared from unmodified birch kraft pulp, was reported to show a pore size of approximately 5 nm and has even been applied for the purpose of organic solvent nanofiltration.[59] Physical characterizations of the film have been thoroughly studied in Lee *et al.* and others.[13,60,61] Highly hydroscopic CNF

provides extremely poor barrier performance, especially in the presence of water vapour, making it alone unsuitable as a packaging material; therefore, we chose this substrate to demonstrate the barrier performance power of a vermiculite-filled nanocomposite. PLA was dissolved at 10 wt% in γ-BL. This solution was mixed with a 5 wt% suspension of vermiculite in the γ-BL/NMF mixture, obtained as described above, at a 50/50 weight ratio of PLA to vermiculite nanosheets. PLA addition does not compromise colloidal stability nor trigger flocculation as evidenced by no significant changes in the SAXS curves upon PLA addition (Fig. S5, ESI†). The nematic character of the mixture was confirmed by birefringence. The suspension with a total solid content (PLA + vermiculite) of 6.7 wt% was coated by doctor blading onto a CNF substrate. A wet coat thickness of 250 μm resulted in a 5 ± 0.5 μm thick dry coating (PLA-verm/CNF) (Fig. S6, ESI†). Due to the porous nature of the CNF substrate, complete solvent removal could be achieved despite the high boiling point of NMF as solvent is allowed to permeate through the substrate while the larger clay particles and polymer chains are not. The area in which solvent molecules have to escape effectively doubles and prevents the trapping of solvent molecules within the coating as the wet layer dries from the outside inwards.

The dried nanocomposite coating resists cracking upon bending due to the highly flexible nanosheets, which is in agreement with previous work on coatings that employ high aspect ratio clay nanosheets.[15] The coating also withstood scratching using a pencil of 2H hardness. For comparison, a CNF paper was coated with only PLA using the same procedure (PLA/CNF).

The oxygen transmission rate (OTR) of the PLA-verm/CNF foil was measured at 23 °C and an elevated 65% relative humidity (RH) and compared to the OTR of both the uncoated CNF paper (35 μm) and the PLA/CNF foil with a coating thickness of 10 μm. OTRs of the neat and the PLA/CNF foils were 13.3 and 13.2 cm^3 m^{-2} day^{-1} atm^{-1}, respectively. A coating layer of PLA on CNF paper has essentially zero effect on the oxygen barrier performance even as a thick coating, as expected, due its exceptionally poor performance even as a bulk material (711 cm^3 m^{-2} day^{-1} atm^{-1}, 25 μm thickness). With or without a PLA coating, CNF oxygen barrier is not suitable for food packaging (Fig. 3a).[62] The use of a PLA-vermiculite nanocomposite coating on CNF is a game-changer in this regard. A dramatic drop in the oxygen transmission rate for the PLA-verm/CNF foil to a value of 1.30 cm^3 m^{-2} day^{-1} atm^{-1} was observed, equating to a barrier improvement factor of 3,484 (eqn (S2), ESI†) and a reduction in oxygen transmission by 90.2% as compared to the neat cellulose paper. This coating brings the oxygen barrier of a paper material (PLA-verm/CNF) into competition with non-degradable and high-performance materials like PVDC and metallized polyethylene terephthalate/polyethylene (PET/Met/PE) laminates, which reports OTR values in the range of 1–2 cm^3 m^{-2} day^{-1} atm^{-1}[63,64] (Fig. 3b). Even more impressive was the drop in the water vapour transmission rate (WVTR) due to the PLA-vermiculite nanocomposite coating. CNF paper, being a hydroscopic substrate, naturally has a poor barrier to water

vapour, especially at an elevated 75% RH, which is well beyond what would be needed for swelling to set in and further deteriorate barrier performance.[65] The neat CNF paper reports a WVTR of 79.6 g m^{-2} day^{-1}, which is slightly improved by the addition of a PLA coating (40.1 g m^{-2} day^{-1}) due to its hydrophobicity, but nevertheless remains unsuitable for demanding food packaging applications. The PLA-verm/CNF foil recorded a dramatically reduced WVTR of 1.74 g m^{-2} day^{-1}, corresponding to a barrier improvement of 91 and a reduction in the CNF transmission rate by 97.8%. Other water soluble, high-barrier polymers like PVOH struggle to maintain WVTR values below 2 g m^{-2} day^{-1} at RH above 50%.[31] With a single degradable coating layer, our PLA-verm/CNF foil again outperforms PET/PE laminates having conventional barrier layers of ethylene vinyl alcohol (EVOH) or PVDC, and rather approaches a WVTR comparable to PET/Met/PE laminates[64] (Fig. 3b). The overall barrier performance of our PLA-verm/CNF foil sits well within the range expected for demanding applications like instant coffee packaging.

The nanocomposite coating imparts such dramatic barrier improvements due to the formation of a 'tortuous path' by impermeable clay nanosheets. The exceptional improvement observed for this vermiculite nanocomposite can be attributed to the preservation of a high aspect ratio during repulsive osmotic delamination and the high degree of orientation of the clay nanosheets that is promoted through solvent casting of osmotically swollen suspensions. These attributes increase the diffusion path of gas molecules, leading to enhanced barrier properties. In addition, the XRD pattern of the nanocomposite coating (Fig. S7, ESI†) indicates the intercalation of the PLA chains within the interlayer space of vermiculite, reflected by the increase in d-spacing from approximately 1.3 nm for butylamine vermiculite to 2.8 nm for the PLA nanocomposite. Previously we have demonstrated that the intercalation of polymer chains can improve the barrier properties of nanocomposite coatings and positively influence the barrier behaviour under increased relative humidity conditions.[32,66] Previous attempts for a CNF nanocomposite film using montmorillonite could not achieve the high performing barrier values that we observed here. Despite a non-biodegradable cross-linked PVOH and poly(acrylic acid) polymer matrix that inherently has better barrier properties than PLA, without the use of a completely delaminated and high aspect ratio filler, the range of achievable barrier performance is limited.[67]

Our method for vermiculite nanocomposites makes bio-based and sustainable materials like cellulose paper a viable option for even ambitious food packaging applications like crispy snacks or instant coffee packaging. While other platy fillers of synthetic origin are expensive and not environmentally benign, vermiculite is provided in bulk by nature for an appealing low price, rendering it attractive for high-volume applications such as food packaging. The coated foil also fulfills consumer preference for transparent packaging (Fig. 3c). The haze and clarity of the coated CNF is improved relative to the uncoated CNF substrate, although transparency decreases slightly from 91.7% to 85.1% for the PLA-verm/CNF foil (Fig. S7, ESI†).
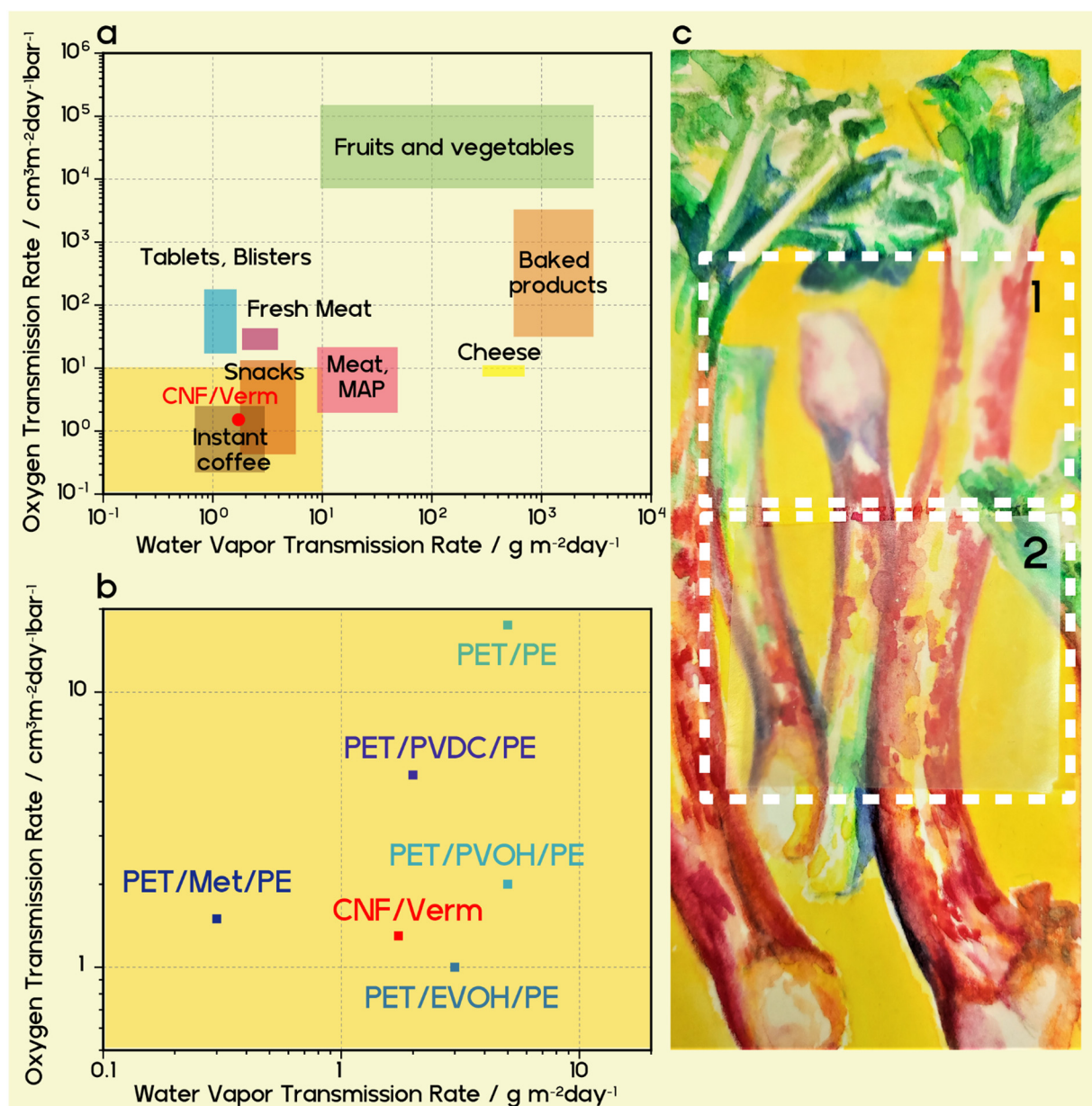
Fig. 3 Barrier properties of nanocomposites. (a) Barrier requirements for packaging of selected foods according to [62], and the barrier properties of PLA-verm/CNF foil. (b) OTR and WTR of commercial non-biodegradable high-performance multilayer packaging according to [64] in comparison with our PLA-verm/CNF foil. (c) Painting covered with the CNF substrate foil (1) and the PLA-verm/CNF foil (2).

High-performance food packaging plays a role in reducing food waste by extending the shelf life of packaged items. To explore the real life consequences of water transmission rate values, we can consider 500 g of a powdered food item (*e.g.* flour) that has a density of 1 g cm^{-3} and initial moisture content of 2 wt% with a critical moisture content of 8 wt% at which the food is regarded spoiled. This food item is packaged in a 3 cm × 15 cm × 10 cm rectangular plastic film pack that is exposed to 75% RH at 23 °C. If the film pack were to be made of neat CNF, the corresponding shelf life would be only 9 days. With a neat 10 μm PLA coating on CNF, the shelf life would be 18 days, making it only suitable for short-term use. Our PLA-verm/CNF foil has the shelf life of an outstanding 416 days,

opening up opportunities for long-term packaging applications (detailed calculation provided in ESI†).[68,69] Such a shelf life extension has dramatic implications on the ability of biodegradable materials to not only reduce the amount of plastic waste entering the environment, but also to reduce food waste and contribute to a more sustainable food production cycle.

Conclusions

Our studies suggest that the modification procedure for vermiculite delamination and transfer to organic solvents provides the ideal nanosheet filler for biodegradable food packaging.

These nanosheets simultaneously addresses two major problems facing widespread implementation of biodegradable polymers: poor barrier properties and high price. Our estimation suggests that the price of 1 kg of delaminated vermiculite on the lab scale is below 1 USD, which is cheaper than PBSA or PLA ($3.5 and $2 per kg in 2019). In this way, we resolve difficulties in the implementation of biodegradable materials by employing a strategy that the packaging industry already uses for commodity polymers, in which almost half of the mass of material consists of inert filler (carbon black or $CaCO_3$) to decrease the price of the final product. A nanocomposite with 50 wt% vermiculite is expected to have a price close to $2 per kg for PBSA and $1.5 per kg for PLA, making it comparable to polyethylene and polypropylene, which are commonly used in the packaging industry.

Experimental section

Materials

Unless otherwise stated, all the chemicals used in the present work were purchased from Sigma Aldrich and directly used without further purification. Butylamine (99.5%), phosphoric acid (≥ 85 wt% in H_2O), sulphuric acid (95.0–98.0%), hydrochloric acid (37 wt% in H_2O), NMF. Citric acid (99%), formic acid (99%), glacial acetic acid (99%).

The PBSA used in this work was purchased from Mitsubishi Chemicals (BioPBS FD92PM). PLA was supplied by Nature Works, USA as the Ingeo 4043D grade semi-crystalline poly-L-lactide.

Mechanically disintegrated CNF was prepared from bleached birch kraft pulp obtained from the Finnish pulp mill. The pulp suspension was pre-refined in a Masuko grinder (Supermasscolloider MKZA10-15J, Masuko Sangyo Co., Japan) at 1500 rpm and fluidized with six passes through a Microfluidizer (Microfluidics M-7115-30 Microfluidicis Corp.) at 1800 bar. Self-standing CNF films were produced by solvent casting method and they were manufactured on a semipilot scale Coatema Coating Machinery GmbH with the patented method.[61,70,71] A 1.6 wt% CNF dispersion, including sorbitol (30 wt% solids in dry film from Sigma), was casted on polypropylene substrate. After evaporation of water, the CNF film with a thickness of 35 μm was separated from the plastic substrate and cut into A4 sheets. The grammage and density of the CNF film is 60 g m^{-2} and 0.93 g cm^{-3}, respectively.

Starting material was Eucatex vermiculite. The structural formula of half unit cell is $[Mg_{0.35}]^{inter}[Mg_{2.475} Al_{0.075} Fe_{0.305} Ti_{0.04}Mn_{0.005}]^{oct}[Si_{3.11} Al_{0.89}]^{tet}O_{10}H_2$ and cation exchange capacity of 147 m equiv./100 g. Natural vermiculite flakes were ground into crystals of 50 μm size. A larger crystal size impedes swelling.

Preparation of ion exchange solutions

Butylamine was titrated in Millipore water to pH = 7 with appropriate acid to obtain the desired counter anion. The solutions were diluted to 1 mol L^{-1}.

Ion exchange procedure. 2 g of the clay was suspended in 200 mL of a 1 M solution of the organic salt (>25-fold excess of the CEC, delamination is prevented by the high ionic strength) and refluxed for 12 h. Then the clay was washed 5 times with 50/50 vol% water/ethanol mixture and dried in the vacuum oven at 70 °C.

Delamination experiment

A known amount of ion-exchanged vermiculite powder was added to 10 mL of MilliQ water in a 15 mL centrifuge tube and was equilibrated in an overhead shaker for 24 h. The vermiculite was then centrifuged at 3000 g for 10 minutes, and the supernatant with the delaminated nanosheets was poured into a Petri dish with a known weight. The water from the supernatant was completely evaporated at 120 °C, and then the Petri dish was equilibrated at 43% RH for 24 h. After weighing the Petri dish, the delamination yield was determined by the ratio between the weight of the nanosheets left after evaporation to the initial weight of vermiculite added for the delamination experiment.

SAXS measurements

SAXS data was collected with a "Double Ganesha AIR" (SAXSLAB, Denmark). In this laboratory-based system, a focused X-ray beam is provided by a rotating copper anode (MicoMax 007HF, Rigaku Corporation, Japan). A position-sensitive detector (PILATUS 300 K, Dectris) was used in different positions to cover the range of the scattering vector $q = 0.004$–0.6 Å^{-1}. Before the measurement, the clay suspensions were added to 1 mm glass capillaries (Hilgenberg, code 4007610). The circularly averaged data was normalized to the incident beam, sample thickness, and measurement time. The scattering of a solvent filled capillary was used for background subtraction. Further evaluation was done with the software Scatter (version 2.5).[72] The measurements for ESI† are performed in vacuum at room temperature on a Xeuss 3.0 (Xenocs SAS, Grenoble, France) equipped with a Cu Kα source (wave length of $\lambda = 1.54$ A) and a Dectris EIGER 2R 1M detector. Different sample to detector distances (50, 350, 900, 1200 and 1800 mm) were used to cover a wider range of scattering vectors q.

AFM measurements

The surface topography has been determined by atomic force microscopic measurements. The images were acquired with a Dimension Icon (Bruker Nano Inc.) in PeakForce tapping mode in air. ScanAsyst Air cantilever (Bruker Nano Inc.) with a typical spring constant of 0.4 N m^{-1} and a resonant frequency of 70 kHz was used. The PeakForce amplitude was 60 nm and the PeakForce frequency was 2 kHz. The AFM images were processed with NanoScope Analysis 1.80 (Bruker Nano Inc.). The topography was flattened by subtracting a first-order polynominal background using a threshold to exclude platelets from flattening. Platelet heights were determined by means of 'step tool' in NanoScope Analysis software. The samples were prepared by slow evaporation of a few drops of a diluted suspension (0.02 g L^{-1}) on a Si-wafer under ambient conditions.

Particle size distribution

Particle size distribution was recorded by static light scattering (SLS) of aqueous dispersions using a Retsch Horiba LA-950 SLS instrument. The refractive index of the solid phase was set to a value of 1.5. A measurement routine called "mica in water" supplied by the manufacturer (Horiba) was applied. The routine determines transmission rates and optimizes the concentration of the suspensions.

Scanning electron microscopy (SEM). SEM images of the cross-section of the film were observed using a ZEISS LEO 1530 (Carl Zeiss AG, Germany) operating at 3 kV.

Foil fabrication

PLA-vermiculite solution was prepared by mixing 2.5 g of a 10 wt% PLA solution in γ-BL with 5 g of a 5 wt% vermiculite dispersion in a γ-BL/NMF (90 : 10) mixture. Total solid content was 6.67 wt%. This solution was mixed overnight on an overhead mixer before being coated onto a CNF substrate using a doctor blading unit (Zehntner ZAA 2300, Zehntner GmbH Testing Instruments, Switzerland). The substrate temperature was 60 °C, the blade speed was 1.5 cm s^{-1}, and the blade height was 250 μm. For the PLA/CNF foil, the PLA solution was coating directly onto the CNF foil using the same conditions. The coated foils were dried overnight at room temperature then in 40 °C oven for two days. Complete solvent removal was confirmed using thermal gravimetric analysis (Fig. S9, ESI†).

Coating thickness of 5 μm was determined using a high-accuracy Digimatic micrometer (Mitutoyo, Japan) with a measuring range of 0–25 mm and a resolution of 0.0001 mm. Thickness was also confirmed with SEM imaging (Fig. S6, ESI†).

Oxygen transmission rates (OTR)

OTR was determined on a Mocon OX-TRAN 2/21 M10x system (Mocon Inc., USA) with a lower detection limit of 5×10^{-4} cm^3 m^{-2} day^{-1} atm^{-1}. The measurements were performed at 23 °C and 65% RH. A mixture of 98 vol% nitrogen and 2 vol% hydrogen was used as the carrier gas and pure oxygen as the permeant ($>$99.95%, Linde Sauerstoff 3.5).

Water vapor transmission rates (WVTR)

WVTR was determined on a HiBarSens HBS 2.0 HT (Sempa Systems GmbH, Dresden, Germany) with a lower detection limit of 10^{-6} g m^{-2} day^{-1}. The tests were conducted at 23 °C at a relative humidity of 75%.

Thermal gravimetric analysis (TGA)

Thermogravimetric analysis was performed at a TG 209 F1 Libra (Netzsch). Approximately 8 mg of the sample was precisely weighed into an aluminum crucible (Concavus) by the internal balance of the machine. The sample was measured in the range of 25–600 °C under nitrogen. The program Proteus Analysis version 8.0 was used to process the results.

X-Ray diffraction (XRD)

XRD patterns were obtained on a Bragg–Brentano-type diffractometer (Empyrean, Malvern Panalytical BV, The Netherlands) equipped with a PIXcel-1D detector using Cu Kα radiation ($\lambda = 1.54187$ Å). All patterns were analyzed using Malvern Panalyticals's HighScore Plus software.

Optical properties

Transmittance, haze, and clarity were measured on a BYK-Gardner Haze-Gard Plus (BYK-Gardner GmbH, Germany). An average of five measurements per film sample were taken.

Author contributions

Conflicts of interest

There are no conflicts to declare.

Acknowledgements

Notes and references

1 Food wastage footprint Impacts on natural resources, Food and Agriculture Organization of the United Nations, 2013.
2 S. Atkinson and I. Payne, A Throwaway World: the challenge of plastic packaging and waste, **https://www.ipsos.com/en/throwaway-world-challenge-plastic-packaging-and-waste**, 2022).
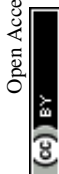
3 Single-Use Plastics Prohibition Regulations, https://www.gazette.gc.ca/rp-pr/p1/2021/2021-12-25/html/reg2-eng.html, 2022).

4 Single-use plastics, https://ec.europa.eu/environment/topics/plastics/single-use-plastics_en, 2022).

5 C. J. Moore, *Environ. Res.*, 2008, **108**, 131–139.

6 N. D. Steenis, E. van Herpen, I. A. van der Lans, T. N. Ligthart and H. C. M. van Trijp, *J. Cleaner Prod.*, 2017, **162**, 286–298.

7 F. Riedewald, E. Wilson, Y. Patel, D. Vogt, I. Povey, K. Barton, L. Lewis, T. Caris, S. Santos and M. O'Mahoney, *Waste Manage.*, 2022, **138**, 172–179.

8 M. C. Heller, S. E. M. Selke and G. A. Keoleian, *J. Ind. Ecol.*, 2018, **23**, 480–495.

9 M. van Birgelen, J. Semeijn and M. Keicher, *Environment and Behavior*, 2008, **41**, 125–146.

10 H. Shaghaleh, X. Xu and S. Wang, *RSC Adv.*, 2018, **8**, 825–842.

11 G. de Souza, M. N. Belgacem, A. Gandini and A. J. F. Carvalho, *Cellulose*, 2021, **28**, 1617–1632.

12 P. Willberg-Keyrilainen, J. Vartiainen, J. Pelto and J. Ropponen, *Carbohydr. Polym.*, 2017, **170**, 160–165.

13 I. Leppänen, M. Vikman, A. Harlin and H. Orelma, *J. Polym. Environ.*, 2019, **28**, 458–470.

14 J.-W. Rhim, H.-M. Park and C.-S. Ha, *Prog. Polym. Sci.*, 2013, **38**, 1629–1652.

15 C. Habel, M. Schöttle, M. Daab, N. J. Eichstaedt, D. Wagner, H. Bakhshi, S. Agarwal, M. A. Horn and J. Breu, *Macromol. Mater. Eng.*, 2018, **303**, 1800333.

16 R. L. Timmins, A. Kumar, M. Röhrl, K. Havlíček, S. Agarwal and J. Breu, *Macromol. Mater. Eng.*, 2021, 2100727, DOI: 10.1002/mame.202100727.

17 Y. Cui, S. Kumar, B. Rao Kona and D. van Houcke, *RSC Adv.*, 2015, **5**, 63669–63690.

18 B. Tan and N. L. Thomas, *J. Membr. Sci.*, 2016, **514**, 595–612.

19 F. Wu, M. Misra and A. K. Mohanty, *Prog. Polym. Sci.*, 2021, **117**, 101395.

20 S. Singha and M. S. Hedenqvist, *Polymers*, 2020, **12**(5), 1095.

21 M. Stöter, D. A. Kunz, M. Schmidt, D. Hirsemann, H. Kalo, B. Putz, J. Senker and J. Breu, *Langmuir*, 2013, **29**, 1280–1285.

22 L. J. Michot, I. Bihannic, S. Maddi, S. S. Funari, C. Baravian, P. Levitz and P. Davidson, *Proc. Natl. Acad. Sci. U. S. A.*, 2006, **103**, 16101–16104.

23 M. Daab, N. J. Eichstaedt, A. Edenharter, S. Rosenfeldt and J. Breu, *RSC Adv.*, 2018, **8**, 28797–28803.

24 M. Daab, N. J. Eichstaedt, C. Habel, S. Rosenfeldt, H. Kalo, H. Schießling, S. Förster and J. Breu, *Langmuir*, 2018, **34**, 8215–8222.

25 J. E. F. C. Gardolinski and G. Lagaly, *Clay Miner.*, 2005, **40**, 547–556.

26 W. J. Roth, T. Sasaki, K. Wolski, Y. Song, D.-M. Tang, Y. Ebina, R. Ma, J. Grzybek, K. Kałahurska, B. Gil, M. Mazur, S. Zapotoczny and J. Cejka, *Sci. Adv.*, 2020, **6**, eaay8163.

27 L. Wang and T. Sasaki, *Chem. Rev.*, 2014, **114**, 9455–9486.

28 P. Davidson, C. Penisson, D. Constantin and J.-C. P. Gabriel, *Proc. Natl. Acad. Sci. U.S.A.*, 2018, **115**, 6662–6667.

29 J.-C. P. Gabriel, F. Camerel, B. J. Lemaire, H. Desvaux, P. Davidson and P. Batail, *Nature*, 2001, **413**, 504–508.

30 R. Liu, T. Gong, K. Zhang and C. Lee, *Sci. Rep.*, 2017, **7**, 1–9.

31 E. S. Tsurko, P. Feicht, C. Habel, T. Schilling, M. Daab, S. Rosenfeldt and J. Breu, *J. Membr. Sci.*, 2017, **540**, 212–218.

32 T. Schilling, C. Habel, S. Rosenfeldt, M. Röhrl and J. Breu, *ACS Applied Polymer Materials*, 2020, **2**, 3010–3015.

33 V. Dudko, K. Ottermann, S. Rosenfeldt, G. Papastavrou and J. Breu, *Langmuir*, 2021, **37**, 461–468.

34 T. J. Brown, N. E. Idoine, C. E. Wrighton, E. R. Raycraft, S. F. Hobbs, R. A. Shaw, P. Everett, E. A. Deady and C. Kresse, *World Mineral Production 2015–2019*, British Geological Survey, Nottingham, UK, 2021.

35 H. Kalo, M. W. Möller, D. A. Kunz and J. Breu, *Nanoscale*, 2012, **4**, 5633–5639.

36 A. Meunier, *Clay Miner.*, 2006, **41**, 551–566.

37 S. Taruta, R. Obara, N. Takusagawa and K. Kitajima, *J. Mater. Sci.*, 2005, **40**, 5597–5602.

38 M. Daab, S. Rosenfeldt, H. Kalo, M. Stöter, B. Bojer, R. Siegel, S. Förster, J. Senker and J. Breu, *Langmuir*, 2017, **33**, 4816–4822.

39 W. G. Garrett and G. F. Walker, *Clays Clay Miner.*, 1960, **9**, 557–567.

40 G. F. Walker and W. G. Garrett, *Science*, 1967, **156**, 385–387.

41 J. A. Rausell-Colom and P. S. Salvador, *Clay Miner.*, 1971, **9**, 139–149.

42 L. F. Braganza, R. J. Crawford, M. V. Smalley and R. K. Thomas, *Clays Clay Miner.*, 1990, **38**, 90–96.

43 J. L. Pérez-Rodríguez, F. Carrera, J. Poyato and L. A. Pérez-Maqueda, *Nanotechnology*, 2002, **13**, 382–387.

44 S. Rosenfeldt, M. Stöter, M. Schlenk, T. Martin, R. Q. Albuquerque, S. Förster and J. Breu, *Langmuir*, 2016, **32**, 10582–10588.

45 M. J. Wilson, *Clay Miner.*, 1999, **34**, 7–25.

46 J.-J. Shao, K. Raidongia, A. R. Koltonow and J. Huang, *Nat. Commun.*, 2015, **6**, 1–7.

47 B. Rotenberg, J.-P. Morel, V. Marry, P. Turq and N. Morel-Desrosiers, *Geochim. Cosmochim. Acta*, 2009, **73**, 4034–4044.

48 K. N. Pearce, *Aust. J. Chem.*, 1980, **33**, 1511–1517.

49 J. W. Bunting and K. M. Thong, *Can. J. Chem.*, 1970, **48**(11), 1654–1656.

50 N. T. Skipper, A. K. Soper and J. D. C. McConnell, *J. Chem. Phys.*, 1991, **94**, 5751–5760.

51 L. Boldon, F. Laliberte and L. Liu, *Nano Rev.*, 2015, **6**(1), 25661.

52 E. Paineau, I. Bihannic, C. Baravian, A.-M. Philippe, P. Davidson, P. Levitz, S. S. Funari, C. Rochas and L. J. Michot, *Langmuir*, 2011, **27**, 5562–5573.

53 D. Goossens, *Sedimentology*, 2008, **55**, 65–96.

54 P. Das, J.-M. Malho, K. Rahimi, F. H. Schacher, B. Wang, D. E. Demco and A. Walther, *Nat. Commun.*, 2015, **6**, 1–14.

55 J. Barthel, R. Buchner and B. Wurm, *J. Mol. Liq.*, 2002, **98–99**, 51–69.

56 C. M. Hansen, *Hansen Solubility Parameters*, CRC Press, 2007.

57 K. Missoum, P. Sadocco, J. Causio, M. N. Belgacem and J. Bras, *Mater. Sci. Eng., C*, 2014, **45**, 477–483.

58 M. Lassoued, F. Crispino and E. Loranger, *Carbohydr. Polym.*, 2021, **254**, 117411.
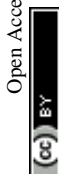
59 A. Mautner, K. Y. Lee, P. Lahtinen, M. Hakalahti, T. Tammelin, K. Li and A. Bismarck, *Chem. Commun.*, 2014, **50**, 5778–5781.

60 K.-Y. Lee, T. Tammelin, K. Schulfter, H. Kiiskinen, J. Samela and A. Bismarck, *ACS Appl. Mater. Interfaces*, 2012, **4**, 4078–4086.

61 T. Mäkelä, M. Kainlauri, P. Willberg-Keyriläinen, T. Tammelin and U. Forsström, *Microelectron. Eng.*, 2016, **163**, 1–6.

62 H. C. Langowski, Presented in part at the Permeation durch Packstoffe, Freising, 2008.

63 J. E. Samuels, *High-barrier flexible polyvinylidene chloride composite applications*, ASTM International, 1986.

64 J. Lange and Y. Wyser, *Packag. Technol. Sci.*, 2003, **16**, 149–158.

65 M. Putkonen, P. Sippola, L. Svrd, T. Sajavaara, J. Vartiainen, I. Buchanan, U. Forsstrm, P. Simell and T. Tammelin, *Philos. Trans. R. Soc., A*, 2018, **376**, 20170037.

66 M. Röhrl, L. K. S. Federer, R. L. Timmins, S. Rosenfeldt, T. Dörres, C. Habel and J. Breu, *ACS Appl. Mater. Interfaces*, 2021, **13**, 48101–48109.

67 S. Spoljaric, A. Salminen, N. Dang Luong, P. Lahtinen, J. Vartiainen, T. Tammelin and J. Seppälä, *Polym. Compos.*, 2014, **35**, 1117–1131.

68 G. L. Robertson, *Food packaging: principles and practice*, CRC press, 2005.

69 G. L. Robertson, *Food packaging and shelf life: a practical guide*, CRC Press, 2009.

70 T. Tammelin, A. Harlin, M. Vehviläinen, P. Nousiainen and K. Kolppo, *BioResources*, 2011, **6**, 2386–2398.

71 T. Tammelin, A. Salminen and U. Hippi, *WIPO (PCT)*, WO2013/060934, 2012.

72 S. Förster, S. Fischer, K. Zielske, C. Schellbach, M. Sztucki, P. Lindner and J. Perlich, *Adv. Colloid Interface Sci.*, 2011, **163**, 53–83.